

Experimental and computational studies on (*Z*)-1-((4-phenylamino)phenylamino)-methylene)naphthalen-2(1*H*)-one

Gökhan Alpaslan · Mustafa Macit ·
Ahmet Erdönmez · Orhan Büyükgüngör

Received: 26 November 2010 / Accepted: 20 January 2011 / Published online: 4 February 2011
© Springer Science+Business Media, LLC 2011

Abstract The Schiff base compound (*Z*)-1-((4-phenylamino)phenylamino)methylene)naphthalen-2(1*H*)-one has been synthesized and characterized by IR, UV–Vis, and X-ray single-crystal determination. Molecular geometry from X-ray experiment of the title compound in the ground state have been compared using the Hartree–Fock (HF) and density functional method (B3LYP) with 6–31G(d,p) basis set. Calculated results show that density functional theory DFT and HF can well reproduce the structure of the title compound. Using the time-dependent density functional theory (TD-DFT) and Hartree–Fock (TD-HF) methods, electronic absorption spectra of the title compound have been predicted and a good agreement with the TD-DFT method and experimental ones is determined. The energetic behavior of the title compound in solvent media has been examined using B3LYP method with the 6–31G(d,p) basis set by applying the polarizable continuum model (PCM). The total energy of the title compound decreases with increasing polarity of the solvent. In addition, DFT calculations of the title compound, molecular electrostatic potential (MEP), natural bond orbital analysis (NBO), and non-linear optical (NLO) properties were performed at B3LYP/6–31G(d,p) level of theory.

Keywords Schiff base · DFT · HF · NBO · Non-linear optical

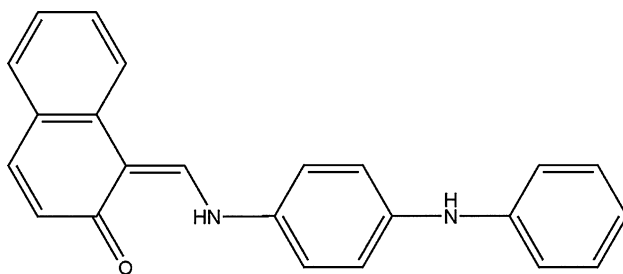
Introduction

Schiff base compounds have received special attention due to their interesting thermochromism and/or photochromism [1, 2], biological properties [3, 4], as well as a variety of potential applications, e.g., for optical data storage [1, 2, 5], as nonlinear optical materials [6, 7], anticorrosive materials [8], or anticancer medicines [9–11]. Tautomerism and isomerism phenomena for these compounds are of particular chemical and theoretical interest in the context of their photochromic and thermochromic properties [2, 12]. Photo- and thermochromism due to a change in the π -electron configuration induced by proton transfer [13, 14]. Such proton exchanging materials can be utilized for the design of various molecular electronic devices [15]. In general, Schiff bases display two possible tautomeric forms, the phenol-imine (or benzenoid) and the keto-amine (or quinoid) forms. Depending on the tautomers, two types of intramolecular hydrogen bonds are observed in Schiff bases: O–H···N in phenol-imine [16, 17] and N–H···O in keto-amine [18–20] tautomers. Another form of Schiff base compounds is their zwitterionic tautomer, which is rarely seen for hydroxy derivatives. The characteristic property of this form is the presence of ionic $\text{N}^+–\text{H}–\text{O}^-$ hydrogen bond [21]. Investigation of structural stability of compounds by both experimental techniques and theoretical methods has been of great interest. Functional material design, theoretical modeling of drug design and so on, has become possible as results of the development of the computational techniques. Many important properties such as molecular orbitals, electrostatic potentials, dipole moment, non-linear optical properties, and vibrational frequencies can be predicted by various computational techniques [22, 23].

In this work, we reported the synthesis, characterization and crystal structure of the Schiff base compound (*Z*)-1-

G. Alpaslan (✉) · A. Erdönmez · O. Büyükgüngör
Department of Physics, Faculty of Arts & Science, Ondokuz
Mayis University, 55139 Kurupelit-Samsun, Turkey
e-mail: gokhana@omu.edu.tr

M. Macit
Department of Chemistry, Faculty of Arts & Science, Ondokuz
Mayis University, 55139 Kurupelit-Samsun, Turkey



Scheme 1 (*Z*)-1-((4-phenylamino)phenylamino)methylene)naphthalen-2(1*H*)-one ($C_{23}H_{18}N_2O$)

((4-phenylamino)phenylamino)methylene)naphthalen-2(1*H*)-one (Scheme 1) as well as the theoretical studies on it using the HF/6–31G(d,p) and DFT/B3LP/6–31G(d,p) methods. The properties of the structural geometry, molecular electrostatic potential (MEP), natural bond analysis (NBO), and non-linear optical properties for the title compound at B3LP/6–31G(d,p) level were studied. These studies are valuable for providing insight into molecular properties of Schiff base compounds.

Experimental and computational method

Synthesis

The compound (*Z*)-1-((4-phenylamino)phenylamino)methylene)naphthalen-2(1*H*)-one was prepared by reflux a mixture of a solution containing 2-hydroxy-1-naphthaldehyde (17.2 mg; 0.1 mmol) in 30 ml ethanol and a solution containing *N*-phenyl-*p*-phenylenediaminediamine (18.4 mg, 0.1 mmol) in 20 ethanol. The reaction mixture was stirred for 2 h under reflux. The crystals of (*E*)-1-((4-chlorophenylamino)methyl)naphthalen-2-ol for X-ray analysis were obtained from ethyl alcohol by slow evaporation (yield 72%; m.p. 385–388 K). The IR spectrum was recorded in the 4000–400 cm^{-1} region using KBr pellet on a Schmadzu FTIR-8900 spectrophotometer. Electronic absorption spectrum was measured on a Unicam UV–VIS spectrophotometer in ethanol.

Crystal data for the title compound

A red crystal of the compound with dimensions of $0.37 \times 0.19 \times 0.03$ mm was mounted on goniometer and data collection was performed on a STOE IPDS II diffractometer by the *w* scan technique using graphite monochromated Mo K α radiation ($\lambda = 0.71073 \text{ \AA}$) at 296 K. The systematic absences and intensity symmetries indicated the monoclinic $Pna2_1$ space group. A total of 12,478 reflections (1,940 unique) with $1.8^\circ < \theta < 26^\circ$

were collected in the *w* scan mode and cell parameters were determined by using X-AREA software [24]. Absorption correction ($\mu = 0.08 \text{ mm}^{-1}$) was obtained by the integration method via X-RED32 software [24]. The crystal structure was solved by direct methods using SHELXS-97 [25]. The absolute configuration could not be determined from X-ray data, as no strong anomalous scatterer is present, 1588 Friedel pairs were merged before the final refinement. The maximum peaks and deepest hole observed in the final $\Delta\rho$ map were 0.12 and -0.13 e \AA^{-3} , respectively. The scattering factors were taken from SHELXL-97 [24]. The molecular graphics were done using *Ortep-3* for Windows [26]. The data collection conditions and parameters of refinement process are listed in Table 1.

Table 1 Crystallographic data for the title compound

Crystal data	
Chemical formula	$C_{23}H_{18}N_2O$
Crystal shape/color	Shapeless/red
Formula weight	338.39
Crystal system	Orthorhombic
Space group	$Pna2_1$
Unit cell parameters	$a = 13.0688(8) \text{ \AA}$ $b = 22.5362(13) \text{ \AA}$ $c = 6.0975(3) \text{ \AA}$
Volume	$1795.84(17) \text{ \AA}^3$
Z	4
$D_x (\text{Mg cm}^{-3})$	1.252
$\mu (\text{mm}^{-1})$	0.08
F_{000}	712
Crystal size (mm^3)	$0.37 \times 0.19 \times 0.03$
Data collection	
Diffractometer/meas. meth	STOE IPDS II/ <i>w</i> -scan
Absorption correction	Integration
T_{\min}	0.978
T_{\max}	0.996
No. of measured, independent and observed reflections	12,478, 1,940, 798
Criterion for observed reflections	$I > 2\sigma(I)$
R_{int}	0.138
θ_{\max}	26
Refinement	
Refinement on	F^2
$R[F^2 > 2\sigma(F^2)], wR, S$	0.055, 0.087, 0.86
No. of reflections	1,940
No. of parameters	242
Weighting scheme	$w = 1/[\sigma^2(F_0^2) + (0.0843P)^2]$ $P = (F_0^2 + 2F_c^2)/3$
$\Delta\rho_{\max}, \Delta\rho_{\min} (\text{e \AA}^{-3})$	0.12, -0.13

Computational methods

The molecular geometry is directly taken from the X-ray diffraction experimental results without any constraints. In the next step, the DFT calculations with a hybrid functional B3LYP (Becke's three parameter hybrid functional using the LYP correlation functional) with the 6–31G(d,p) basis set and Hartree–Fock calculations with the 6–31G(d,p) basis set using Berny method [27, 28] were performed with the Gaussian 03W software package [29] and Gaussview visualization program [30]. The electronic absorption spectra were calculated using the time-dependent density functional theory (TD-DFT) and Hartree–Fock (TD-HF) methods [31–34]. Also, it is calculated in ethanol solution using the polarizable continuum model (PCM) [35–38]. In order to investigate the energetic and dipole moment behavior of the title compound in solvent media, we also carried out optimization calculations in three kinds of solvents (chloroform, ethanol, and water) by using PCM method. To investigate the reactive sites of the title compound the molecular electrostatic potential was evaluated using the BLYP/6–31G(d,p) method. The molecular electrostatic potential, $V(r)$, at a given point $r(x, y, z)$ in the vicinity of a molecule, is defined in terms of the interaction energy between the electrical charge generated by the molecule's electrons and nuclei and a positive test charge located at r . For the system studied the $V(r)$ values were calculated as described previously using the equation [39],

$$V(r) = \sum_A \frac{Z_A}{R_A - r} - \int \frac{\rho(r')}{r' - r} dr' \quad (1)$$

where Z_A is the charge of nucleus A , located at R_A , $\rho(r')$ is the electronic density function of the molecule, and r' is the dummy integration variable. The linear polarizability and first hyperpolarizability properties of the title compound were obtained from molecular polarizabilities based on theoretical calculations. In addition, NBO analysis was

performed at B3LYP/6–31G (d,p) level by means of the NBO 3.1 program within the Gaussian 03 W package [40].

Results and discussion

Description of the crystal structure

The title compound, an *Ortep-3* view of which is shown in Fig. 1, crystallizes in the orthorhombic space group Pna_2_1 with $Z = 4$ in the unit cell. The asymmetric unit in the crystal structure contains only one molecule. The C11–N1 and C2–O1 bonds of the title compound are the most important indicators of the tautomeric type. X-ray structure determinations reveal that the keto tautomer is favoured over the enol tautomer. This is evident from the observed C11–N1 bond distance of 1.319(7) Å, which is consistent with the C–N single bond; similarly the C2–O1 distance of 1.297(2) Å is also consistent with the C=O double bonding. These bond distances are comparable with those of compounds previously reported as keto-amine [41–43]. In addition to these, the shortened C3–C4 naphthalene ring bond distance of 1.347 (8) Å suggests a quinoidal effect and confirms that the O1–C2 bond is not a pure single bond. The imine N1 atom is sp^2 hybridized and displays coplanarity of the naphthaldimine fragment [44].

The dihedral angles between the naphthalene plane A (C1–C10), the benzene plane B (C12–C17), and the other benzene plane C (C18–C23) are 4.33(14) $^\circ$ (A/B), 30.21 $^\circ$ (A/C), and 29.68 $^\circ$ (B/C). It is also known that Schiff bases may exhibit photochromism depending on the planarity or non-planarity, respectively [45]. The molecular structure is stabilized by a N1–H1…O1 intramolecular hydrogen bond (Table 2) which generates an S(6) ring motif (Fig. 1) [46]. The sum of the Van der Waals radius of the N and O atoms [3.07 Å] is significantly longer than the intramolecular N1…O1 [2.521(7) Å] hydrogen bond length [47]. In the crystal structure, molecules are linked into

Fig. 1 *Ortep-3* diagram of the title compound. Displacement ellipsoids are drawn at the 40% probability level and H atoms are shown as small spheres of arbitrary radii. The intramolecular hydrogen bond is shown as a dashed line

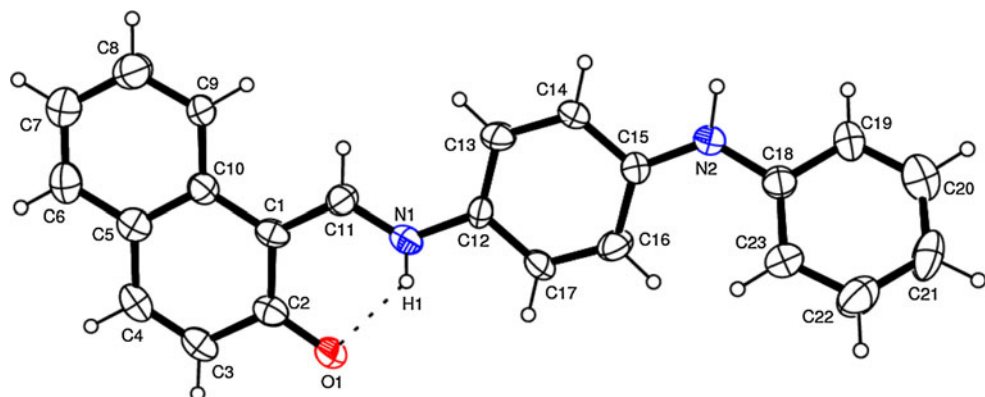
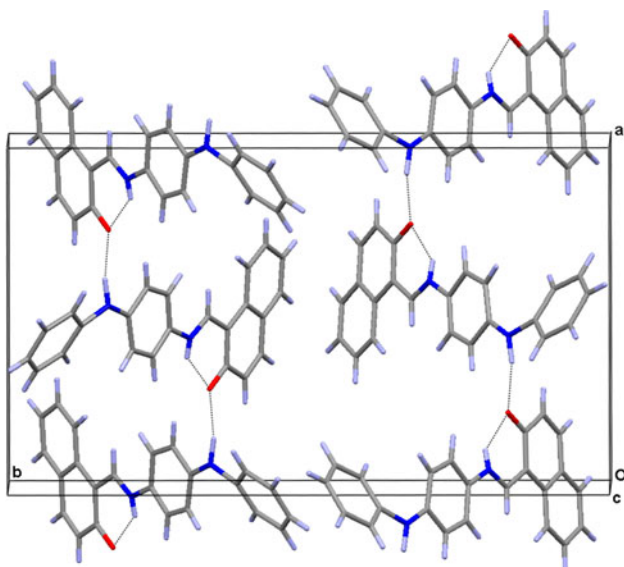


Table 2 Hydrogen-bond geometry (\AA , $^\circ$)

D–H…A	D–H	H…A	D…A	D–H…A
N1–H1…O1	0.74(5)	1.96(6)	2.521(7)	133(7)
N2–H2…O1 ⁱ	0.98(5)	1.93(5)	2.897(6)	168(5)

Symmetry code (i): $x - 1/2, -y + 1/2, z + 1$

**Fig. 2** Packing diagram of the title compound

one-dimensional polymeric C(11) chains along the *a*-axis by intermolecular N2–H1…O1 hydrogen bonds (Fig. 2).

Optimized geometries

The optimized parameters (bond lengths, bond angles, and dihedral angles) of the title compound have been obtained at HF and B3LYP methods with the 6–31G(d,p) basis set. The calculated results are listed in Table 3. When the X-ray structure of the title compound is compared with its optimized counterparts (see Fig. 3), conformational discrepancies are observed between them. The dihedral angles between *A*, *B*, and *C* planes are calculated at 39.17° (*A/B*), 20.30° (*A/C*), 59.26° (*B/C*) for HF, and 11.82° (*A/B*), 54.92° (*A/C*), 43.87° (*B/C*) for B3LYP, respectively. The orientation of the three rings is defined by the torsion angles C1–C11–N1–C12 [-180°], C16–C15–N2–C18 [$-16.4(10)^\circ$] and C14–C15–N2–C18 [$160.4(7)^\circ$] which have been calculated as 178.4° , -22.7° , and 160.1° for B3LYP, and -176.9° , -52.8° , and 130.2° for HF, respectively.

As seen from Table 3, most of the calculated bond lengths and the bond angles are slightly different from the experimental ones. We noted that the experimental results belong to the solid phase and theoretical calculations belong to the gas phase. In the solid state the experimental

Table 3 Selected molecular structure parameters

Parameters	Experimental	HF/ 6–31G(d,p)	B3LYP/ 6–31G(d,p)
<i>Bond lengths</i> (\AA)			
C1–C2	1.422(7)	1.463	1.464
C1–C10	1.443(8)	1.473	1.461
C2–C3	1.439(8)	1.464	1.452
C2–O1	1.297(7)	1.221	1.262
C3–C4	1.347(8)	1.331	1.355
C4–C5	1.420(7)	1.454	1.441
C5–C6	1.407(9)	1.397	1.409
C5–C10	1.409(8)	1.404	1.425
C6–C7	1.351(9)	1.373	1.383
C7–C8	1.401(8)	1.391	1.403
C8–C9	1.376(8)	1.376	1.386
C9–C10	1.398(7)	1.403	1.413
C1–C11	1.406(8)	1.371	1.395
C11–N1	1.319(7)	1.328	1.335
N1–C12	1.416(7)	1.409	1.403
C12–C13	1.376(6)	1.384	1.403
C13–C14	1.376(7)	1.385	1.384
C14–C15	1.409(7)	1.387	1.407
C15–C16	1.411(7)	1.394	1.406
C16–C17	1.370(8)	1.378	1.388
C17–C12	1.384(7)	1.390	1.402
C15–N2	1.371(7)	1.401	1.395
N2–C18	1.405(7)	1.402	1.400
C18–C19	1.391(7)	1.394	1.406
C19–C20	1.362(10)	1.380	1.391
C20–C21	1.353(9)	1.386	1.396
C21–C22	1.370(9)	1.382	1.395
C22–C23	1.376(9)	1.386	1.393
C18–C23	1.384(8)	1.390	1.405
Max. dif.		0.076	0.043
RMSE		0.0043	0.0038
<i>Bond angles</i> ($^\circ$)			
C11–C1–C2	119.1(6)	118.7	118.2
C11–C1–C10	120.6(5)	121.1	121.3
C2–C1–C10	120.3(6)	120.1	120.3
O1–C2–C1	122.6(6)	122.9	122.6
O1–C2–C3	118.9(6)	119.8	119.9
C1–C2–C3	118.5(6)	117.1	117.3
C4–C3–C2	119.9(6)	121.3	121.5
C3–C4–C5	123.7(7)	122.9	122.4
C6–C5–C10	120.0(6)	120.6	120.2
C6–C5–C4	121.8(7)	119.8	120.3
C10–C5–C4	118.2(6)	119.4	119.1
C7–C6–C5	121.7(7)	121.1	121.3
C6–C7–C8	118.1(7)	118.6	118.9
C9–C8–C7	121.9(7)	120.8	120.7

Table 3 continued

Parameters	Experimental	HF/ 6–31G(d,p)	B3LYP/ 6–31G(d,p)
C8–C9–C10	120.3(6)	121.5	121.6
C9–C10–C5	117.9(6)	117.1	117.2
C9–C10–C1	122.7(6)	124.0	123.9
C5–C10–C1	119.5(6)	118.8	118.9
N1–C11–C1	122.0(6)	126.5	123.1
C13–C12–C17	118.2(5)	118.8	118.2
C13–C12–N1	124.9(5)	122.3	123.6
C17–C12–N1	116.7(5)	118.8	117.9
C12–C13–C14	120.7(6)	120.3	120.4
C15–N2–C18	128.8(5)	125.9	129.5
C11–N1–C12	126.8(6)	125.2	128.0
C22–C23–C18	120.3(7)	120.1	120.0
C21–C22–C23	121.3(7)	121.0	121.1
C20–C21–C22	117.6(8)	118.8	118.9
C21–C20–C19	123.3(8)	120.6	120.5
C23–C18–C19	118.2(7)	118.8	118.7
C23–C18–N2	125.7(6)	123.2	122.8
C19–C18–N2	116.0(6)	117.9	118.4
C16–C17–C12	122.1(6)	120.7	121.2
C20–C19–C18	119.2(8)	120.5	120.6
N2–C15–C14	117.1(6)	120.4	118.6
N2–C15–C16	126.6(6)	121.2	123.3
C14–C15–C16	116.2(6)	118.2	117.9
C17–C16–C15	120.6(6)	120.6	120.5
C13–C14–C15	122.0(6)	121.0	121.4
Max. dif.		5.4	3.3
RMSE		0.0289	0.0207
<i>Torsion angles (°)</i>			
C2–C1–C11–N1	1.9(9)	1.7	0.3
C1–C11–N1–C12	−180	−176.9	178.4
C16–C15–N2–C18	−16.4(10)	−52.8	−22.7
N1–C12–C17–C16	179.3(6)	179.9	179.9
C11–C1–C2–O1	−2.5(10)	−3.2	0.8
C19–C18–N2–C15	163.8(7)	168.9	155.0

results are related to molecular packing, but in the gas phase the isolated molecules are considered in the theoretical calculations. The greatest differences of the bond lengths between experimental and the predicted values are found at C20–C21 bond with the difference being 0.043 Å for B3LYP method, and C2–O1 bond with a value 0.076 Å for HF method. For the bond angles, the biggest differences occur at N2–C15–C16 bond angle, with the different values being 3.3° for B3LYP method and 5.4° for HF method. According to these results, the biggest differences of bond lengths and bond angles mainly occurs in the groups involved in the hydrogen bond [i.e., C2–O1, N2–C15–C16]

which can also easily be understood taking into account the intra- and intermolecular hydrogen bond interactions present in the crystal.

In order to compare the theoretical results with the experimental values, root mean square error (RMSE) is used and the values which for the bond lengths and bond angles are calculated as 0.0043 Å and 0.0289° for HF method, and 0.0038 Å and 0.0207° for B3LYP method, respectively. A logical method for globally comparing the structures obtained with the theoretical calculations is by superimposing the molecular skeleton with the obtained X-ray diffraction, giving a RMSE of 0.0136 Å for B3LYP and 0.0483 Å for method HF, respectively (Fig. 3). According to these results, it may be concluded that the B3LYP calculation well reproduce the geometry of the title compound.

IR spectroscopy

FT-IR spectrum of the title compound was recorded in the 4000–400 cm^{−1} region using KBr pellet on a Schmadzu FT-IR 8900 spectrophotometer. The some characteristic bands of the stretching vibrations of the NH, N–H···O, CN, and CO groups were observed. The IR spectrum of the title compound shows two bands at 3300 and 3112 cm^{−1} due to N–H stretching vibrations. These differences between N–H stretching vibration frequencies are because of the intramolecular N–H···O hydrogen bonding which leads a shift to lower wave-number. The weak bands in the range 3033–3000 cm^{−1} correspond to the symmetric and asymmetric stretching vibrations of aromatic CH bonds. The characteristic region of 1500–1700 cm^{−1} can be used to identify the proton transfer of Schiff bases [48]. The title compound shows a strong band at 1620 cm^{−1} which is assigned to C=O stretching vibration [49]. In addition to these, the C–N stretching vibration was observed at 1315 cm^{−1}. The absorption bands in the 1550–1590 cm^{−1} region must be related to the keto structure (C=C external double bond). In other words, these bands occur only if there is a considerable amount of the keto-tautomer [50]. The presence of N–H, C=O, and C–N stretching vibrations strongly suggest that the title compound has keto-amine tautomeric character in the solid state.

Electronic absorption spectra

The UV–Vis electronic absorption spectrum of the title compound was recorded within 200–600 nm range on a Unicam UV–Vis spectrophotometer in EtOH solvent. The observed spectrum showed three bands at 466 nm ($\log \varepsilon = 4.093$), 316 nm ($\log \varepsilon = 3.839$), and 256 nm ($\log \varepsilon = 4.126$), which correspond to keto-amine and phenol-imine forms, respectively. These values are similar

Fig. 3 Atom-by-atom superimposition of the structures calculated (**a** DFT, **b** HF) over the X-ray structures (blue) for the title compound (Color figure online)

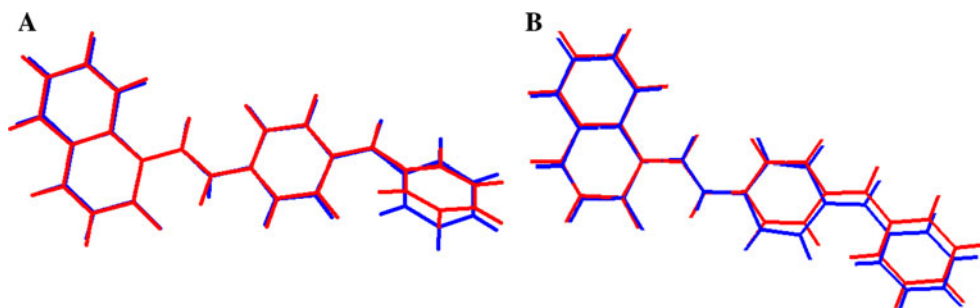
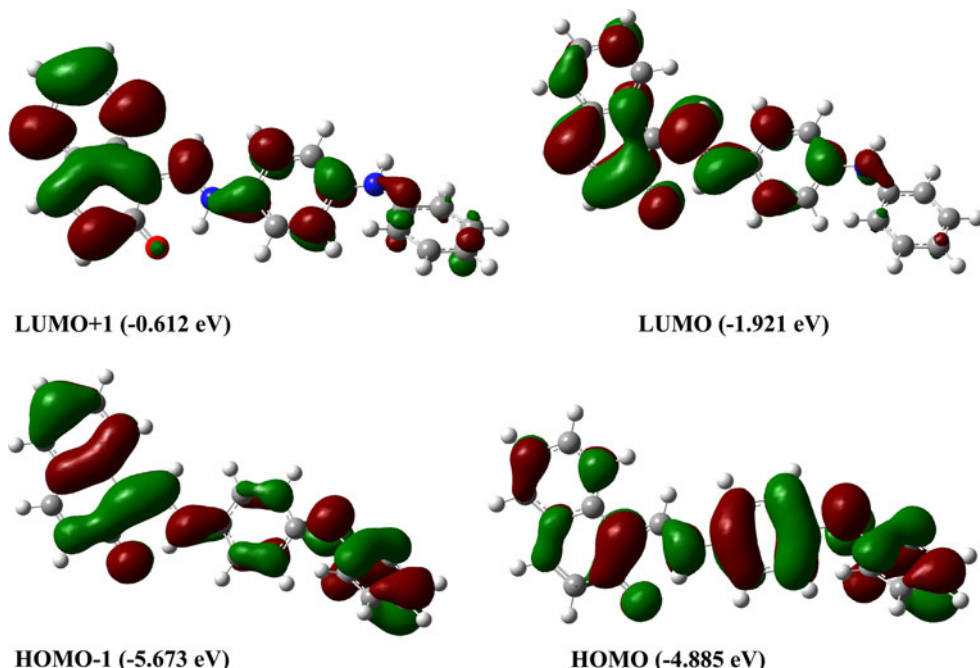


Fig. 4 Molecular orbital surfaces and energy levels given in parentheses for the LUMO+1 (−0.612 eV), LUMO (−1.921 eV), HOMO−1 (−5.673 eV), and HOMO (−4.885 eV) of the title compound computed at B3LYP/6–31G(d,p) level



to those found in related compound. [21] The electronic absorption spectra of 2-hydroxy Schiff bases which exist mainly as phenol-imine structure indicate the presence of a band at <400 nm, whereas compounds that existing in the keto-amine form show a new band, especially in polar and nonpolar solvents at >400 nm [50–53]. According to these results, the keto-amine character is dominant in ethanol solvent which has absorption band at 466 nm.

Electronic absorption spectra of the title compound were calculated by TD-DFT and TD-HF methods based on the structure gas phase, respectively. For the TD-HF calculations, the absorption wavelengths are obtained at 294, 241, and 175 nm. It is obvious that these bands are not consistent of the experimental results. Besides that, the TD-DFT theoretical absorption band calculations obtained at 438, 309, and 238 nm and it can be seen that these values are corresponding to the experimental absorption ones. In addition to the results gas phase, TD-DFT calculations of the title compound in ethanol solvent were performed by using PCM model. The PCM calculations reveal that the

calculated absorption bands have red shift at 472, 323, and 281 nm when compared with the gas-phase calculations of TD-DFT method. The reason for this red shift is solvent effect which can affect the geometry and electronic structure as well as the properties of the molecule as solvent effects induce the lower energy of the molecules, and generate more significant red shift for absorption bands [54, 55]. Comparing these values with the corresponding experimental values, TD-DFT method for both in gas-phase and solvent media is useful to predict UV–Vis spectrum.

According to the investigation on the frontier molecular orbital (FMO) energy levels of the title compound, we can find that the corresponding electronic transfer happened between the highest occupied molecular orbital (HOMO) and the lowest unoccupied molecular orbital (LUMO), HOMO and LUMO+1, HOMO−1 and LUMO+1 orbitals, respectively. Figure 4 shows the distributions and energy levels of the FMOs computed at the B3LYP/6–31G(d,p) level for the title compound.

Table 4 Calculated energies, dipole moments, and frontier orbital energies

	Gas phase ($\varepsilon = 1$)	Chloroform ($\varepsilon = 4.9$)	Ethanol ($\varepsilon = 24.55$)	Water ($\varepsilon = 78.39$)
E_{total} (Hartree)	−1072.0617547	−1072.07841139	−1072.08560718	−1072.08836333
E_{HOMO} (eV)	−4.935	−4.892	−4.885	−4.872
E_{LUMO} (eV)	−1.833	−1.889	−1.921	−1.908
ΔE (eV)	3.102	3.002	2.964	2.961
μ (D)	4.0564	5.4584	6.0996	6.3201

As seen from Fig. 4, in the LUMO+1 and LUMO, electrons are mainly delocalized naphthalene ring and the atoms of imine group; in the HOMO−1 and HOMO, electrons are delocalized on the whole structure. Molecular orbital coefficients analyses based on optimized geometry indicate that, for the title compound, the frontier molecular orbitals are mainly composed of π -atomic orbitals, so the electronic transitions are mainly derived from the contribution of bands $\pi-\pi^*$.

Total energies in solvent media

In order to evaluate the energetic behavior of the title compound in solvent media, we carried out calculations in three kinds of solvent (water, ethanol, chloroform). Total molecular energies, frontier molecular orbital energies and dipole moments have been calculated in solvent media with B3LYP/6–31G(d,p) level using PCM model and the results are presented in Table 4. According to Table 4, we can infer that obtained total molecular energies and energy gap (ΔE) between the HOMO–LUMO of the title compound by PCM method decreases with the increasing polarity of the solvent and while the dipole moments will increase with the increase of the polarity of the solvent. Solvent effects improve the charge delocalized in the molecules, therefore, inducing the dipole moments to be raised. Ground-state dipole moment is an important factor in measuring solvent effect a large ground-state dipole moment gives rise to strong solvent polarity effects [56, 57].

Molecular electrostatic potential

MEP is related to the electronic density and is a very useful descriptor in determining sites for electrophilic and nucleophilic reactions as well as hydrogen bonding interactions [58, 59]. The electrostatic potential $V(r)$ is also well suited for analyzing processes based on the “recognition” of one molecule by another, as in drug–receptor and enzyme–substrate interactions, because it is through their potentials that the two species first “see” each other [60, 61].

To predict reactive sites of electrophilic and nucleophilic attack for the investigated molecule, the MEP at the B3LYP/6–31G(d,p) optimized geometry was calculated.

The negative (red) region of MEP was related to electrophilic reactivity and the positive (blue) region to nucleophilic reactivity (see Fig. 5). Negative region is chiefly on the O1 atom. The negative $V(r)$ value is −0.0572 a.u. for O1 atom. However, a maximum positive region is localized on the N2–H2 bond with a value of +0.0572 a.u., indicating a possible site for nucleophilic attack. These sites give information concerning the region from where the compound can have metallic bondings and intermolecular interactions. The MEP is best suited for identifying sites for intra- and intermolecular interactions [62]. So, Fig. 5 confirms the existence of the intermolecular N2–H2···O1 interactions.

NBO analysis

NBO analysis provides an efficient method for studying intra- and intermolecular bonding and interaction among bonds, and also provides a convenient basis for investigating charge transfer or conjugative interaction in molecular systems [63]. The larger the $E^{(2)}$ value, the more intensive is the interaction between electron donors and electron acceptors, i.e., the more donating tendency from electron donors to electron acceptors and the greater the extent of conjugation of the whole system. Delocalization of electron density between occupied Lewis-type (bond or lone pair) NBO orbitals and formally unoccupied (antibond or Rydberg) non-Lewis NBO orbitals correspond to a stabilizing donor–acceptor interaction. In order to investigate the intra and intermolecular interactions, the stabilization energies of the title compound were performed by using second-order perturbation theory. For each donor NBO(i) and acceptor NBO(j), the stabilization energy $E^{(2)}$ associated with electron delocalization between donor and acceptor is estimated as [64, 65]

$$E^{(2)} = -q_i \frac{(F_{ij})^2}{\varepsilon_j - \varepsilon_i} \quad (2)$$

where q_i is the donor orbital occupancy, ε_i , ε_j are diagonal elements (orbital energies), and F_{ij} is the off-diagonal NBO Fock matrix element. The results of second-order perturbation theory analysis of the Fock Matrix at B3LYP/6–31G(d,p) level of theory are presented in Table 5.

Fig. 5 Molecular electrostatic potential map calculated at B3LYP/6–31G(d,p) level
(Color figure online)

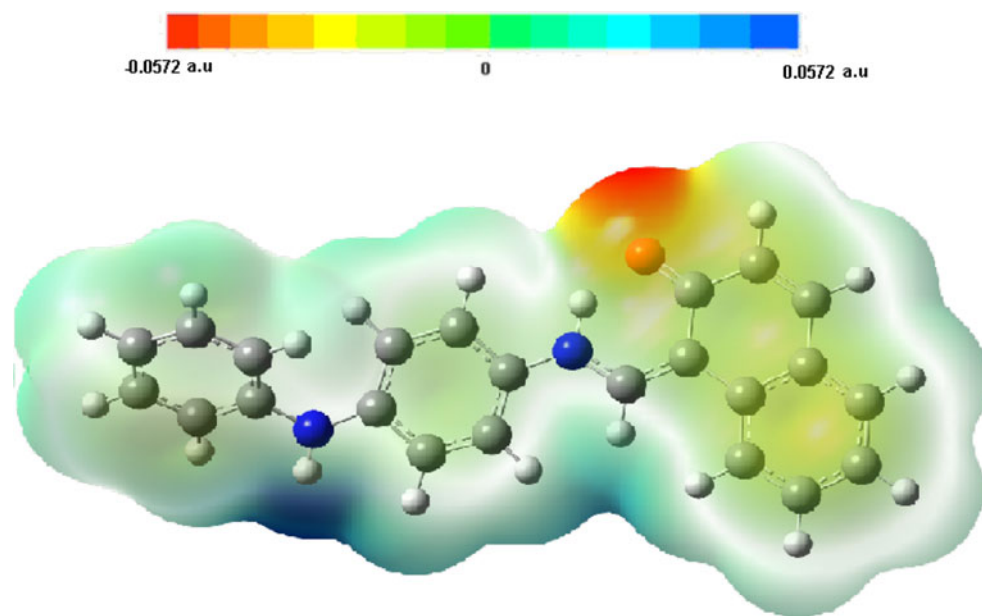


Table 5 Second-order perturbation theory analysis of the Fock matrix in NBO basis, calculated at B3LYP/6–31G(d,p) level

Donor orbital (<i>i</i>)	Acceptor orbital (<i>j</i>)	$E^{(2)}^{\text{a}}$ (kcal/mol)	$\epsilon_j - \epsilon_i^{\text{b}}$ (a.u.)	F_{ij}^{c} (a.u.)
LP(1) O1	BD(1) N1–H1	6.26	1.06	0.074
LP(2) O1	BD(1) N1–H1	28.92	0.73	0.131
LP(1) O1	BD(1) N2–H2	3.71	1.17	0.059
LP(2) O1	BD(1) N2–H2	0.67	0.76	0.021
LP(3) O1	BD(1) N2–H2	1.23	0.74	0.031

^a $E^{(2)}$ means energy of hyper conjugative interactions

^b Energy difference between donor and acceptor *i* and *j* NBO orbitals

^c F_{ij} is the Fock matrix element between *i* and *j* NBO orbitals

NBO analysis revealed the $n(\text{O1}) \rightarrow \sigma(\text{N1–H1})$ interactions give the strongest stabilization to the system of the title compound by 35.18 kcal mol⁻¹, and strengthen the intramolecular N1–H1…O1 hydrogen bond. The lone pairs of O1 also donate its electrons to σ -type antibonding orbital for N2–H2. The total stabilization energy of N2–H1…O1 intermolecular hydrogen bonding is 5.61 kcal mol⁻¹. Thus, it is apparent that N–H…O intermolecular hydrogen bond significantly influence crystal packing in this molecule.

Non-linear optical effects

Non-linear optical (NLO) effects arise from the interactions of electromagnetic fields in various media to produce new fields altered in phase, frequency, amplitude, or other propagation characteristics from the incident fields [66]. NLO is at the forefront of current research because of its importance in providing the key functions of frequency shifting, optical modulation, optical switching, optical logic, and optical memory for the emerging technologies in areas such as telecommunications, signal processing, and

optical interconnections [67–70]. Organic molecules that exhibit extended π conjugation, in particular, show enhanced second-order NLO properties [71].

The total static dipole moment (μ), the linear polarizability (α), and the first hyperpolarizability (β) using the *x*, *y*, *z* components are defined as [72, 73]:

$$\mu = \sqrt{\mu_x^2 + \mu_y^2 + \mu_z^2} \quad (3)$$

$$\alpha = \frac{\alpha_{xx} + \alpha_{yy} + \alpha_{zz}}{3} \quad (4)$$

$$\beta = \sqrt{(\beta_{xxx} + \beta_{xxy} + \beta_{xzz})^2 + (\beta_{yyy} + \beta_{xxy} + \beta_{yzz})^2 + (\beta_{zzz} + \beta_{xxz} + \beta_{yyz})^2} \quad (5)$$

The dipole moment (μ), linear polarizability (α), and the first hyperpolarizability (β) were calculated at the B3LYP/6–31G(d,p) level using Gaussian 03W program package. The calculated dipole moment (μ), polarizability (α), and first hyperpolarizability (β) for title compound are 4.0564 D, 49.54 Å³, and 100.029×10^{-30} cm⁵/esu, respectively. The calculated values of first hyperpolarizability

and polarizability are greater than that of 4-(2,3,4-trihydroxybenzylideneamino)antipyrine [66] and 2-methyl-6-[2-(trifluoromethyl)phenyl-iminomethyl]phenol [73]. These results indicate that title compound is a good candidate of nonlinear optical material.

Conclusion

(Z)-1-((4-Phenylamino)phenylamino)methylene)naphthalen-2(1*H*-one has been synthesized and characterized by IR, UV–Vis, and X-ray single-crystal diffraction. The X-ray, IR, and UV–Vis spectral data for the title compound show that the compound exists in the keto-amine tautomeric form, which is stabilized by the intramolecular N–H…O hydrogen bond. The comparisons between the calculated results and the X-ray experimental data indicate that B3LYP method is better than HF method in evaluating geometric parameters. The TD-DFT calculations lead to a very closer agreement with the experimental absorption spectra both gas phase and solvent media. Molecular orbital coefficient analyses suggest that the electronic spectrum corresponds to the $\pi \rightarrow \pi^*$ electronic transition. The total energy of the title compound decreases with increasing polarity of the solvent. The MEP map shows that the negative potential site is on oxygen atom while the positive potential sites are around the hydrogen atoms. These sites give information about the region from where the compound can have intermolecular interactions and metallic bonding. The NBO analysis revealed that the $n(O1) \rightarrow \sigma$ (N1–H1) interaction gives the strongest stabilization to the system, and the major interaction for the intermolecular O1…N2 contact is $n(O1) \rightarrow \sigma$ (N2–H2). This study also demonstrates that the title compound can be used as a good nonlinear optical material.

Supplementary data

CCDC-795577 contains the supplementary crystallographic data for the compound reported in this paper. These data can be obtained free of charge at www.ccdc.cam.ac.uk/conts/retrieving.html [or from the Cambridge Crystallographic Data Centre (CCDC), 12 Union Road, Cambridge CB2 1EZ, UK; fax: +44 1223 336033; e-mail: deposit@ccdc.cam.ac.uk].

References

1. Hadjoudis E (1995) Mol Eng 5:301
2. Hadjoudis E, Mavridis IM (2004) Chem Soc Rev 33:579
3. Mezler CM, Cahil A, Mezler DE (1980) J Am Chem Soc 102:6075
4. Hill MP, Carroll EC, Toney MNT, Larsen DS (2008) J Phys Chem B 112:5867
5. Feringa BL, Jager WF, de Lange B (1993) Tetrahedron 49:8267
6. Karakas A, Elmali A, Ünver H, Svoboda I (2004) J Mol Struct 702:103
7. Behpour M, Ghoreishi SM, Soltani N, Salavati-Niasari M, Hamadanian M, Gandomi A (2008) Corros Sci 50:2172
8. Shelley MD, Hartley L, Paul PW, Fish RG (2000) Anticancer Drug 11:209
9. Napier I, Ponka P, Richardson DR (2005) Blood 105:1867
10. Vicini P, Geronikaki A, Incerti M, Busonera B, Pomi G, Cabras CA, La Colla P (2003) Bioorg Med Chem 11:4785
11. Dziembowska T, Szafran M, Katrusiak A, Rozwadowski Z (2009) J Mol Struct 929:32
12. Trzesowska-Kruszynska A (2010) Struct Chem 21:131
13. Hadjoudis E, Vitterakis M, Mavridis IM (1987) Tetrahedron 43:1345
14. Xu X-X, You X-Z, Sun Z-F, Wang X, Liu H-X (1994) Acta Crystallogr C 50:1169
15. Alarcon SH, Pagani D, Bacigalupo J, Olivieri AC (1999) J Mol Struct 475:233
16. Petek H, Albayrak Ç, Ağar E, Ocak Iskeleli N, Şenel I (2007) Acta Crystallogr E 63:o810
17. Özak A, Albayrak Ç, Odabaşoğlu M, Büyükgüngör O (2007) Acta Crystallogr C 63:o177
18. Karabiyik H, Ocak Iskeleli N, Petek H, Albayrak Ç, Ağar E (2008) J Mol Struct 873:130
19. Koşar B, Büyükgüngör O, Albayrak Ç, Odabaşoğlu M (2004) Acta Crystallogr C 60:o458
20. Tanak H, Erşahin F, Koysal Y, Ağar E, Işık Ş, Yavuz M (2009) J Mol Mod 15:1281
21. Petek H, Albayrak Ç, Odabaşoğlu M, Şenel I, Büyükgüngör O (2010) Struct Chem 21:681
22. Zhang Y, Guo ZJ, You XZ (2001) J Am Chem Soc 123:9378
23. Alpaslan Y, Süleymanoğlu N, Öztekin E, Erşahin E, Ağar E, Işık Ş (2010) J Chem Crystallogr 40:950
24. Stoe Cie (2002) X-AREA (Version 1.18) and X-RED32 (Version 1.04). Darmstadt, Germany
25. Sheldrick GM (2008) Acta Crystallogr A 64:112
26. Farrugia LJ (1997) J Appl Crystallogr 30:565
27. Schlegel HB (1982) J Comput Chem 3:214
28. Peng C, Ayala PY, Schlegel HB, Frisch MJ (1996) J Comput Chem 17:49
29. Frisch MJ, Trucks GW, Schlegel HB, Scuseria GE, Robb MA, Cheeseman JR, Montgomery JA Jr, Vreven T, Kudin KN, Burant JC, Millam JM, Iyengar SS, Tomasi J, Barone V, Mennucci B, Cossi M, Scalmani G, Rega N, Petersson GA, Nakatsuji H, Hada M, Ehara M, Toyota K, Fukuda R, Hasegawa J, Ishida M, Nakajima T, Honda Y, Kitao O, Nakai H, Klene M, Li X, Knox JE, Hratchian HP, Cross JB, Bakken V, Adamo C, Jaramillo J, Gomperts R, Stratmann RE, Yazyev O, Austin AJ, Cammi R, Pomelli C, Ochterski JW, Ayala PY, Morokuma K, Voth GA, Salvador P, Dannenberg JJ, Zakrzewski VG, Dapprich S, Daniels AD, Strain MC, Farkas O, Malick DK, Rabuck AD, Raghavachari K, Foresman JB, Ortiz JV, Cui Q, Baboul AG, Clifford S, Cioslowski J, Stefanov BB, Liu G, Liashenko A, Piskorz P, Komaromi I, Martin RL, Fox DJ, Keith T, Al-Laham MA, Peng CY, Nanayakkara A, Challacombe M, Gill PMW, Johnson B, Chen W, Wong MW, Gonzalez C, Pople JA (2004) Gaussian 03, Revision E.01. Gaussian Inc., Wallingford
30. Frisch A, Dennington R II, Keith T, Millam J, Nielsen AB, Holder AJ, Hiscock J (2007) GaussView reference, version 4.0. Gaussian Inc., Pittsburgh
31. Runge E, Gross EKU (1984) Phys Rev Lett 52:997

32. Stratmann RE, Scuseria GE, Frisch MJ (1998) *J Chem Phys* 109:8218
33. Bauernschmitt R, Ahlrichs R (1996) *Chem Phys Lett* 256:454
34. Casida ME, Jamorski C, Casida KC, Salahub DR (1998) *J Chem Phys* 108:4439
35. Miertus S, Scrocco E, Tomasi J (1981) *Chem Phys* 55:117
36. Barone V, Cossi M (1998) *J Phys Chem A* 102:1995
37. Cossi M, Rega N, Scalmani G, Barone V (2003) *J Comput Chem* 24:669
38. Tomasi J, Mennucci B, Cammi R (2005) *Chem Rev* 105:2999
39. Politzer P, Murray J (2002) *Theor Chem Acc* 108:134
40. Glendening ED, Badenhoop JK, Reed AE, Carpenter JE, Weinhold F (1995) NBO version 3.1. Theoretical Chemistry Institute, University of Wisconsin, Madison
41. Petek H, Albayrak Ç, Odabaşoğlu M, Şenel İ, Büyükgüngör O (2008) *J Chem Crystallogr* 38:901
42. Temel E, Ağar E, Büyükgüngör O (2010) *Acta Crystallogr E* 66:o1131
43. Ünver H, Yıldız M, Kiraz A, Özgen Ö (2009) *J Chem Crystallogr* 39:17
44. Pavlovic G, Sosa JM (2000) *Acta Crystallogr C* 56:o1117
45. Mavridis IM, Hadjoudis E, Mavridis A (1978) *Acta Crystallogr B* 34:3709
46. Bernstein J, Davies RE, Shimoni L, Chang NL (1995) *Angew Chem Int Ed Engl* 34:1555
47. Bondi A (1964) *J Phys Chem* 68:441
48. Alpaslan G, Tanak H, Ağar AA, Erdönmez E, Işık § (2010) *Struct Chem* 21:1027
49. Ünver H, Zengin DM, Güven K (2000) *J Chem Crystallogr* 30:359
50. Salman SR, Saleh NAI (1997) *Spectrosc Lett* 30:1289
51. Yıldız M, Kılıç Z, Hökelek T (1998) *J Mol Struct* 441:1
52. Ünver H, Yıldız M, Zengin DM, Özbeý S, Kendi E (2001) *J Chem Crystallogr* 31:211
53. Tanak H, Ağar A, Yavuz M (2010) *J Mol Mod* 16:577
54. Rong ZC, Jiang LZ, Hong CY, Shan CH, Zhi WY, Hua YL (2009) *J Mol Struct (Theochem)* 899:86
55. Tanak H, Alaman AA, Yavuz M (2009) *Int J Quant Chem.* doi: [10.1002/qua.22504](https://doi.org/10.1002/qua.22504)
56. Masternak A, Wenska G, Milecki J, Skalski B, Franzen S (2005) *J Phys Chem* 109:759
57. Le Y, Chen JF, Pu M (2008) *Int J Pharm* 358:214
58. Scrocco E, Tomasi J (1978) *Adv Quantum Chem* 11:115
59. Luque FJ, Lopez JM, Orozco M (2000) *Theor Chem Acc* 103:343
60. Politzer P, Laurence PR, Jayasuriya K, McKinney J (1985) *Environ Health Perspect* 61:191
61. Scrocco E, Tomasi J (1973) *Topics in current chemistry*, vol 7. Springer, Berlin, p 95
62. Politzer P, Concha MC, Murray JS (2000) *Int J Quant Chem* 80:184
63. Snehalatha M, Ravikumar C, Hubert Joe I, Sekar N, Jayakumar VS (2009) *Spectrochim Acta A* 72:654
64. Schwenke DW, Truhlar DG (1985) *J Chem Phys* 82:2418
65. Gutowski M, Chalasinski G (1993) *J Chem Phys* 98:4728
66. Sun YX, Hao QL, Wei WX, Yu ZX, Lu LD, Wang X, Wang YS (2009) *J Mol Struct THEOCHEM* 904:74
67. Andraud C, Brotin T, Garcia C, Pelle F, Goldner P, Bigot B, Collet A (1994) *J Am Chem Soc* 116:2094
68. Geskin VM, Lambert C, Bredas JL (2003) *J Am Chem Soc* 125:15651
69. Nakano M, Fujita H, Takahata M, Yamaguchi K (2002) *J Am Chem Soc* 124:9648
70. Sajan D, Joe H, Jayakumar VS, Zaleski J (2006) *J Mol Struct* 785:43
71. Thanthiriwatte SK, Nalin de Silva KM (2002) *J Mol Struct THEOCHEM* 617:169
72. Zhang R, Du B, Sun G, Sun YX (2010) *Spectrochim Acta A* 75:1115
73. Tanak H (2010) *J Mol Struct THEOCHEM* 950:5